ACS APPLIED MATERIALS & INTERFACES

Research Article

www.acsami.org

Hollow Core–Shell Structured Ni–Sn@C Nanoparticles: A Novel Electrocatalyst for the Hydrogen Evolution Reaction

Leiming Lang,[‡,§] Yi Shi,[†] Jiong Wang,[†] Feng-Bin Wang,[†] and Xing-Hua Xia*[,†]

[†]State Key Laboratory of Analytical Chemistry for Life Science, School of Chemistry and Chemical Engineering, Collaborative Innovation Center of Chemistry for Life Sciences, Nanjing University, 22 Hankou Road, Nanjing 210093, P. R. China

[‡]Environmental Science College, Nanjing Xiaozhuang University, Nanjing 211171, P. R. China

Supporting Information

ABSTRACT: Pt-free electrocatalysts with high activity and low cost are highly pursued for hydrogen production by electrochemically splitting water. Ni-based alloy catalysts are potential candidates for the hydrogen evolution reaction (HER) and have been studied extensively. Here, we synthesized novel hollow core–shell structure Ni–Sn@C nanoparticles (NPs) by sol–gel, chemical vapor deposition, and etching processes. The prepared electrocatalysts with porous hollow carbon layers have a high conductivity and large active area, which exhibit good electrocatalytic activity toward HER. The Tafel slope of ~35 millivolts per decade measured in acidic solution for Ni–Sn@C NPs is the smallest one to date for the Ni–Sn alloy catalysts, and exceeds those of the most non-noble metal catalysts, indicating a possible Volmer–Heyrovsky reaction mechanism. The synthetic method can be extended to prepare other hollow core–shell structure electrocatalysts for low-temperature fuel cells.

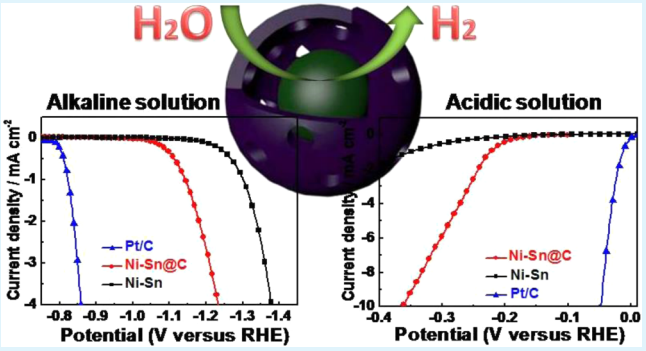

KEYWORDS: *core–shell structure, Ni–Sn, porous carbon, electrocatalysis, hydrogen evolution reaction*

1. INTRODUCTION

In recent years, more attention has been paid to hydrogen energy because it is one of the cleanest and most efficient energy carriers for the future.[1−4] The demand for hydrogen will probably continue to increase with the energy shortage. The efficient pathway to produce hydrogen is electrochemical reduction of water where hydrogen evolution reaction (HER) is a key step. It is generally accepted that platinum is considered as the most efficient catalyst for the HER,[5,6] but its high cost and scarcity hamper large-scale applications, which encourages us to exploit Pt-free catalysts with high activity and low cost.

The alloying materials of two (or more) metals have the presented interesting and promising characteristics as desirable catalysts for HER. According to the well-known "volcano" curve,[7] nickel is an appropriate candidate because of the high catalytic activity and abundance in nature. However, the affinity of nickel to hydrogen is relatively strong, which makes desorption of hydrogen difficult. Alloying the nickel with weaker hydrogen binding energy may balance the adsorption and desorption of hydrogen atoms. Ni-based alloy catalysts including Ni–Sn,[8−12] Ni–Mo,[13−15] Ni–Al,[16] Ni–Fe,[17,18] Ni–P,[19,20] and Ni–Se[21,22] have been verified to show high electrochemical activity in catalyzing the conversion of H_2O to H_2. Among them, tin is a good alternative because of its weaker hydrogen binding as compared to nickel; thus, an accelerated reaction rate for HER can be achieved.

Several approaches to the synthesis of Ni–Sn electrocatalytic cathode materials have been reported in the past years, including electrodeposition,[9−12,22] in situ reduction,[23,24] and high-temperature calcinations.[25,26] However, using these methods aggregation of nanoparticles or formation of bulklike alloy cannot be avoided, which reduce the effective active sites of the catalysts and thus the catalytic activity for HER. Construction of porous hollow core–shell structured materials may effectively overcome the aggregation problem. Porous carbon structure with high conductivity is a promising matrix to separate nanoparticles. In this communication, we report an approach to the synthesis of novel core–shell structured Ni–Sn@C hollow spheres as efficient electrocatalyst for HER. The nanomaterials were carefully characterized. Electrochemical results show that core–shell structured Ni–Sn@C hybrid shows high electrocatalytic activity toward HER in both acidic and alkaline media.

2. EXPERIMENTAL SECTION

2.1. Materials. Poly(vinylpyrrolidone) (PVP-K30, Mn 58 000), tin protochloride dehydrate ($SnCl_2·2H_2O$), nickel nitrate hexahydrate ($Ni(NO_3)_2·2H_2O$), sodium borohydride ($NaBH_4$), triethylene glycol (TEG), tetraethyl orthosilicate (TEOS), and ethanol (≥99.9%) were

Received: January 29, 2015
Accepted: April 14, 2015
Published: April 14, 2015

DOI: 10.1021/acsami.5b00873
ACS Appl. Mater. Interfaces 2015, 7, 9098−9102

purchased from Sigma-Aldrich Chemical Co. Ltd. They were of analytical grade and used without further purification.

2.2. Synthesis of Ni−Sn Nanoparticles. Ni−Sn nanoparticles (NPs) were prepared according to the previous work with some modification.[24] In a typical procedure, PVP (2 g) and $SnCl_2$ (0.26 g) were dissolved in TEG (90 mL) under sonication. The transparent solution bubbled with N_2 was heated to 170 °C under continuous stirring. Then, freshly prepared $NaBH_4$ solution (0.5 g of $NaBH_4$ dissolved in 15 mL of TEG) was added into the mixed solution slowly. After 15 min, $NiCl_2$ solution (0.1 g of $NiCl_2$ dissolved in 8 mL of TEG) was added, and the reaction was maintained at 170 °C for 1.5 h. The product was separated from the reaction mixture by centrifugation and washed with ethanol several times.

2.3. Synthesis of Ni−Sn@C Nanoparticles. The synthetic process of Ni−Sn@C NPs is indicated in Scheme 1. In detail, the

Scheme 1. Illustration for the Synthesis Process of Ni−Sn@C NPs

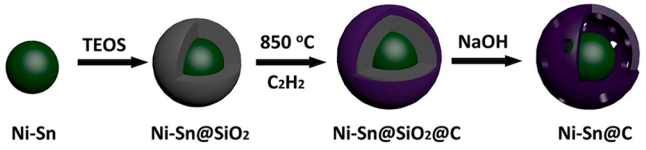

synthesized Ni−Sn NPs were dispersed in 200 mL of ethanol under sonication. Into this dispersion, 2.0 mL of concentrated $NH_3{\cdot}H_2O$ was added under continuous stirring. Then, Ni−Sn@SiO_2 NPs were synthesized by adding a mixture of 20 mL of ethanol and 1 mL of TEOS within 2 h followed by 24 h of reaction under continuous stirring. The separated and dried product was placed into a pipe furnace and calcined in an atmosphere of $Ar/C_2H_2/H_2$ (6:2:2) at 850 °C for 1 h using a ramping rate of 5 °C/min from room temperature.[27] The SiO_2 shell was chemically etched in a solution of 2 M NaOH at 50 °C for 3−6 h. The final Ni−Sn@C NPs were centrifuged and dried in an oven at 110 °C.

2.4. Characterization. The morphology of the products was characterized by scanning electron microscopy (SEM; EDAX-4800) and transmission electron microscopy (TEM; Japan JEOL-2010). The phase purity of the products was characterized by X-ray power diffraction (XRD; Shimadzu XD-3A X-ray diffractometer with Cuα radiation, λ = 0.154 17 nm) at a scan rate of 4°/min in a range from 10° to 80°, and the energy dispersive spectrum (EDS) was recorded on an EDAX-4800. The X-ray photoelectron energy spectrum (XPS) was recorded on a VG ESCALAB MKII. The accelerating voltage and working current were 12.5 kV and 20.0 mA, respectively. The BET (Brunauer−Emmett−Teller) surface area was measured by ASAP2020 (Micromeritics, United States).

2.5. Electrochemical Measurements. Glassy carbon electrode (GCE, diameter of 3 mm) was polished to a mirrorlike surface using 0.05 μm alumina slurry, then rinsed thoroughly with ethanol and water in an ultrasonic bath to remove any alumina residue, and finally dried with blowing N_2 gas. The GCE loaded with 0.10 mg/cm^2 catalysts was used as the working electrode. The catalyst ink was prepared as follows: 5 mg of catalyst was dispersed in 1 mL of ethanol containing 20 μL of 5 wt % Nafion solution (Sigma-Aldrich) using sonication for at least 30 min. Then, 2 μL of the above dispersion was pipetted onto the GCE and dried at room temperature. Electrochemical measurement was performed at room temperature using a three-electrode configuration with a Pt wire and a Ag/AgCl as the counter electrode and the reference, respectively. Cyclic voltammetry (CV) and linear sweep voltammetry (LSV) were conducted on a CHI 660D electrochemical workstation (CHI Inc., USA) at a scan rate of 5 mV·s^{-1} in both acidic and alkaline media. Prior to electrochemical measurements, the electrolyte (0.5 M H_2SO_4 or 1 M NaOH) was degassed by bubbling argon for 30 min. All the potentials refer to the reversible hydrogen electrode (RHE) without specification. For comparison, commercial 5% Pt/C catalyst (Sigma-Aldrich) was used for CV and LSV measurements under the same conditions.

3. RESULTS AND DISCUSSION

The chemical composition and crystal structure of the sample were characterized by X-ray diffraction (XRD) analysis. The XRD patterns of Ni−Sn@C NPs (Figure 1a) and Ni−Sn NPs

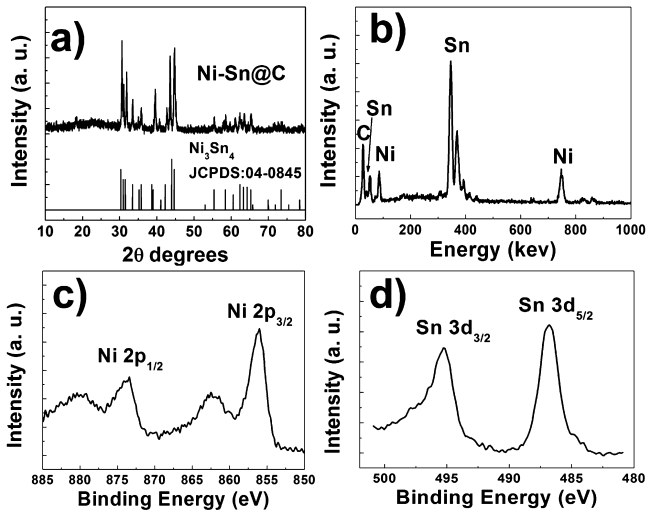

Figure 1. (a) XRD pattern and (b) EDS spectrum of Ni−Sn@C NPs. XPS spectra of the sample: (c) Ni 2p and (d) Sn 3d.

(Supporting Information, Figure S1) show the characteristic diffraction peaks of Ni_3Sn_4, although several diffraction peaks are not in good agreement with the standard XRD pattern (Figure 1a, JCPDS 04−0845). The results are consistent with the ones reported previously.[24] The sample composition is confirmed by EDS (Figure 1b), which reveals that the sample is composed of Ni and Sn elements with the atom percentages of 43% and 67%, respectively, matching well the composition ratio of Ni/Sn = 3:4. The relatively intense signal of C is generated from the decomposition of C_2H_2 gas.

The surface electronic states and the chemical composition of the product were examined by using XPS. The survey XPS curves (Figure 1c,d) reveal that the sample is composed of Ni and Sn, as confirmed by EDS. The binding energies of the Ni $2p_{3/2}$ and $2p_{1/2}$ states are located at 856.0 and 873.4 eV (Figure 1c), respectively, which agree with the value illustrated in the literature.[25] The binding energy of the Sn 3d state occurring at 495.3 and 486.8 eV (Figure 1d) is consistent with the reported ones.[25] Compared with the free Ni−Sn NPs (Supporting Information, Figure S2), slight shifts of the peaks arise in XPS spectra for Ni 2p and Sn 3d of Ni−Sn@C NPs, which demonstrates that the surface of Ni−Sn is oxidized slightly during chemical removal of SiO_2 in NaOH solution. The N_2 adsorption/desorption isotherm in Figure 2 shows a type IV curve with a hysteresis loop. The Brunauer−Emmett−Teller (BET) surface area is ∼78 m^2 g^{-1}, and the pore distribution curve is shown in inset of Figure 2 with peaks at ∼0.5 and 2.5 nm, which demonstrates Ni−Sn@C NPs have different pore structures.

The morphology and microstructure of the samples were observed by SEM and TEM and are presented in Figure 3. The SEM (Figure 3a) and TEM (Figure 3c) images show that the synthesized Ni−Sn NPs with the average diameter of ∼60 nm are not very uniform. After the Ni−Sn NPs were wrapped by SiO_2 layer by sol−gel method, obvious core−shell structure appears (Figure 3d). The thickness of SiO_2 shell is ∼50 nm

DOI: 10.1021/acsami.5b00873
ACS Appl. Mater. Interfaces 2015, 7, 9098−9102

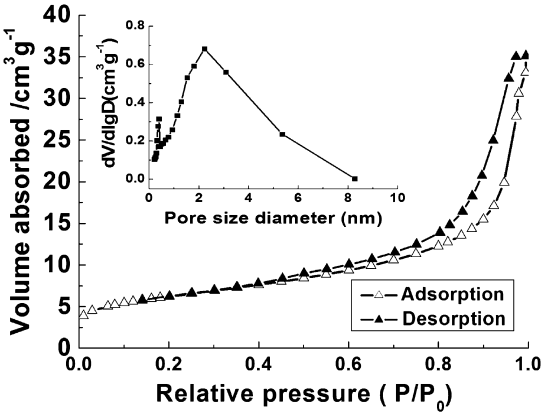

Figure 2. Nitrogen adsorption/desorption isotherm and Barrett–Joyner–Halenda (BJH) pore size distribution plot (inset) of Ni–Sn@C NPs.

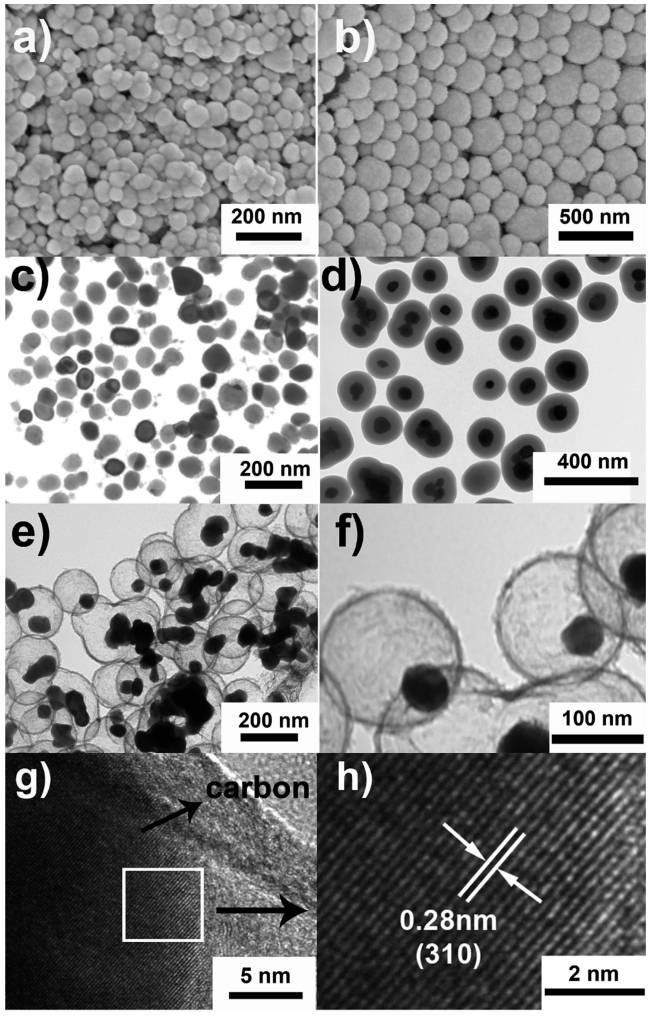

Figure 3. SEM and TEM images of (a, c) Ni–Sn NPs and (b, d) Ni–Sn@SiO_2 NPs, (e) Low-resolution and (f, g) magnified TEM images of Ni–Sn@C NPs. (h) The HRTEM image of Ni–Sn NP as marked with the white frame in (g).

(Figure 3d), and the size of Ni–Sn@SiO_2 NPs (Figure 3b) is significantly larger than the Ni–Sn NPs. The formation of a few large Ni–Sn@SiO_2 NPs is possibly attributed to aggregation of Ni–Sn NPs during shell structure formation. Figure 3e shows the low-magnification TEM image of Ni–Sn@C NPs, clearly showing the hollow core–shell structure. The magnified TEM images (Figure 3f,g) show that the carbon shell has a rough surface and porous structure, which are of importance for mass transport in electrocatalytic performance for HER. Figure 3h is the HRTEM image of the Ni–Sn NP marked with the white frame in Figure 3g, which confirms the high crystallinity of Ni–Sn NP by a visible set of lattice fringes of 0.28 nm, characteristics of the (310) plane of Ni_3Sn_4 in agreement with XRD result. However, the main (111) lattice plane appears in free Ni–Sn NPs (Supporting Information, Figure S3), which is different from Ni–Sn@C NPs. The possible reason is that high calcination changes the crystallinity of Ni–Sn NPs.

In addition, the core–shell structure of Ni–Sn@C NPs can be verified by dark-field TEM image (Figure 4a). The EDS

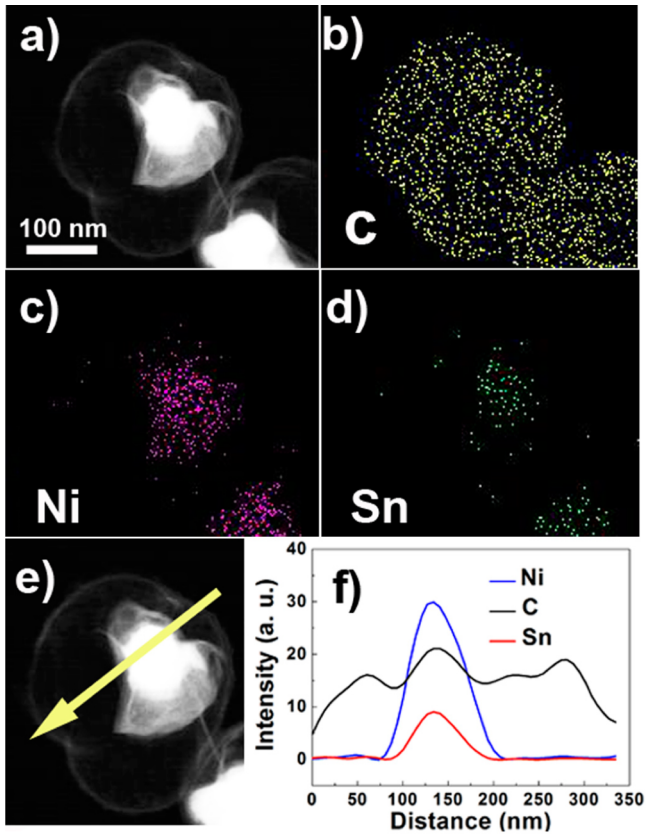

Figure 4. (a, e) Dark-field TEM images and (b, c, d) EDS elemental mapping images of Ni–Sn@C NPs. (f) Compositional line profiles across the single Ni–Sn@C NP along the line marked by arrow in (e).

elemental mapping images indicate the distribution of Ni, Sn, C elements in the Ni–Sn@C NPs clearly (Figure 4b–d). The compositional line profiles across the single Ni–Sn@C NP are shown in Figure 4f. Several peaks and valleys evidence the formation of the hollow core–shell structure.

Electrochemical measurements were performed at room temperature using a three-electrode configuration with a Pt wire and a Ag/AgCl as the counter electrode and the reference, respectively. The GCE loaded with 0.10 mg/cm^2 of catalyst was used as the working electrode. The electrocatalytic performance of the synthesized hollow core–shell structure Ni–Sn@C NPs toward HER was investigated in both N_2-saturated 0.5 M H_2SO_4 and 1 M NaOH solutions. For comparison, the unwrapped Ni–Sn NPs and commercial Pt/C catalyst (5 wt

DOI: 10.1021/acsami.5b00873
ACS Appl. Mater. Interfaces 2015, 7, 9098–9102

%) were also investigated under the same conditions. Figure 5 shows the polarization curves and Tafel plots after *iR* correction

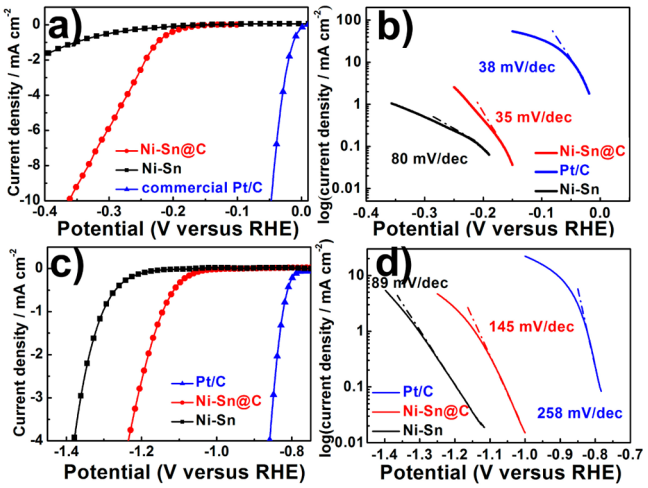

Figure 5. Polarization curves for the HER and corresponding Tafel plots on modified electrodes comprising the Ni–Sn NPs, Ni–Sn@C NPs, and commercial Pt/C catalyst measured in different solutions: (a, b) 0.5 M H_2SO_4 and (c, d) 1 M NaOH solution.

derived in different media for the catalysts. The Ni–Sn@C NPs exhibit high electrocatalytic activity with the onset potential at ca. −170 mV in acidic medium and the corresponding exchange current density of ∼0.14 mA/cm^2 (Figure 5a), which rises rapidly with increasing the overpotential. In contrast, the free Ni–Sn NPs have a low activity for HER with a more negative onset potential and a very small cathodic current density (Figure 5a). As expected, the commercial Pt/C catalyst shows the highest HER activity with a more positive onset potential close to zero (Figure 5a). Tafel analysis of the HER polarization curves (Figure 5b) demonstrates that Ni–Sn@C NPs have a smaller Tafel slope of 35 millivolts per decade than that of the commercial Pt/C catalyst (38 millivolts per decade). In the current work, the observed Tafel slope of 35 millivolts per decade is the smallest one to date for the Ni–Sn alloy catalysts and outperforms those of the most non-noble metal catalysts of MoS_2/graphene (41 millivolts per decade),[2] porous MoS_2 (50 millivolts per decade),[28] Ni_2P (46 millivolts per decade),[19] and Ni/NiO/$CoSe_2$ nanobelts (39 millivolts per decade).[3] The Tafel slope is an inherent property of catalysts for the HER. Close to 40 millivolts per decade indicates a possible Volmer–Heyrovsky reaction mechanism of HER on the Ni–Sn@C NPs electrocatalyst with electrochemical desorption of hydrogen as the rate-limiting step. This demonstrates that Ni–Sn@C NPs have a comparable HER activity to the commercial Pt/C catalyst.

To further assess the intrinsic activity of the catalysts, the electrocatalytic performance was also measured in alkaline solution. As expected, the HER activities of all electrocatalysts decrease, and the onset potentials shift to more negative values than those in acidic solution. As shown in Figure 5c, the onset potentials are ca. −1.17, −1.02, and −0.78 V for the free Ni–Sn NPs, Ni–Sn@C NPs, and commercial Pt/C catalysts, respectively. The measured Tafel slopes (Figure 5d) are larger than those observed in acidic solution. The catalyst with larger Tafel value in alkaline solutions implies that the catalytic reaction undergoes a different HER mechanism as compared to the one in acidic media, involving an additional water dissociation step in the alkaline solution. The durability tests in different media demonstrate Ni–Sn@C NPs exhibit a high cycling stability with a little loss of the cathodic current measured in alkaline solution after 100 cycles (Supporting Information, Figure S4), which is better than those of Ni–Sn NPs both in acidic (Supporting Information, Figure S5) and alkaline solution. The inductively coupled plasma (ICP) results of the final solution after 100 cycles for Ni–Sn@C NPs show that the Ni^{2+} and Sn^{2+} concentration are negligible and both below 0.05 ppm, which demonstrates good stability of Ni–Sn@C NPs in acidic medium.

The observed superior HER activity of Ni–Sn@C NPs over Ni–Sn NPs can be attributed to the following two reasons. First, the Volmer–Heyrovsky reaction mechanism under the acidic conditions can be summarized as the electrochemical hydrogen adsorption ($H_3O^+ + e^- \rightarrow H_{ads} + H_2O$) and hydrogen desorption process ($H_{ads} + H_3O^+ + e^- \rightarrow H_2\uparrow + H_2O$).[2] The Ni–Sn@C NPs with hollow core–shell structure have large surface area and expose more HER active sites compared with the Ni–Sn NPs, which improves the dissociative adsorption of water on the surface of catalysts and contributes to adsorption–desorption process for plenty of hydrogen. Hollow structure also provides a confined space to enhance the HER activity. Additionally, the exposed active lattice plane (310) of Ni–Sn@C NPs is different from that of Ni–Sn NPs, which also contributes to the promoted electrochemical performance of Ni–Sn@C NPs. Second, the carbon shell of Ni–Sn@C NPs not only makes the single Ni–Sn NPs isolate from other particles and avoid aggregating, which favors the long-term cycling stability of the catalyst, but also guarantees better electrical conductivity to promote the exchange of electron, leading to the increase of HER efficiency.

To better understand the electrocatalytic performance of Ni–Sn NPs, oxygen reduction reaction (ORR) was investigated in 0.1 M KOH solution saturated by O_2 at a scan rate of 10 mV s^{-1}. As shown in the polarization curves (Supporting Information, Figure S6a), Ni–Sn NPs exhibited an inefficient two-step ORR process with onset potentials at −0.23 and −0.61 V, which are attributable to the reduction of O_2 to HO_2^- and HO_2^- to OH^-, respectively.[29] Compared with commercial Pt/C catalyst, Ni–Sn@C shows low catalytic activity (Supporting Information, Figure S6b), which indicates that it is not a good electrocatalyst for ORR. We will endeavor to improve the ORR activity of Ni–Sn@C in our future work.

4. CONCLUSIONS

In summary, novel hollow core–shell structured Ni–Sn@C NPs were synthesized by several steps including sol–gel, chemical vapor deposition, and etching processes. The prepared catalyst has the hollow structure and porous carbon layer, which increase both conductivity for electron communication and the electrochemical active surface area of the catalysts. Thus, the Ni–Sn@C NPs show much better HER activity and longer stability than the free Ni–Sn NPs and other Pt-free catalysts, such as MoS_2/graphene, porous MoS_2, Ni_2P, and Ni/NiO/$CoSe_2$. However, the HER activity of the present NiSn@C NP catalysts is still not comparable to that of the commercial Pt catalysts. Thus, future investigation will be focused on the proper designing of highly active core catalysts shelled with porous carbon layer. The present approach can also be extended to synthesize catalysts with core–shell structures for other catalytic oxidation and reduction reactions, especially for ORR, oxidation reactions of small organic

DOI: 10.1021/acsami.5b00873
ACS Appl. Mater. Interfaces 2015, 7, 9098–9102

compounds such as methanol, ethanol, and formic acid for low-temperature fuel cells.

■ ASSOCIATED CONTENT

Supporting Information

XRD pattern, XPS spectra, TEM and HRTEM images, durability test curves of Ni−Sn NPs and Ni−Sn@C NPs, and oxygen reduction polarization curves. This material is available free of charge via the Internet at http://pubs.acs.org.

■ AUTHOR INFORMATION

Corresponding Author

*E-mail: xhxia@nju.edu.cn.

Present Address

[§]State Key Laboratory of Analytical Chemistry for Life Science, School of Chemistry and Chemical Engineering, Collaborative Innovation Center of Chemistry for Life Sciences, Nanjing University, 22 Hankou Road, Nanjing 210093, P. R. China.

Funding

This work is supported by grants from the National 973 Basic Research Program (2012CB933800), the National Natural Science Foundation of China (21035002, 21205059, 21275070, 21327902), the National Science Fund for Creative Research Groups (21121091), and the Natural Science Foundation of Jiangsu province (BK2012071).

Notes

The authors declare no competing financial interest.

■ REFERENCES

(1) Dresselhaus, M. S.; Thomas, I. L. Alternative Energy Technologies. *Nature* **2001**, *414*, 332−337.

(2) Li, Y.; Wang, H.; Xie, L.; Liang, Y.; Hong, G.; Dai, H. MoS_2 Nanoparticles Grown on Graphene An Advanced Catalyst for the Hydrogen Evolution Reaction. *J. Am. Chem. Soc.* **2011**, *133*, 7296−7299.

(3) Xu, Y. F.; Gao, M. R.; Zheng, Y. R.; Jiang, J.; Yu, S. H. Nickel/Nickel(II) Oxide Nanoparticles Anchored onto Cobalt(IV) Diselenide Nanobelts for the Electrochemical Production of Hydrogen. *Angew. Chem., Int. Ed.* **2013**, *52*, 8546−8550.

(4) Gao, M. R.; Xu, Y. F.; Jiang, J.; Yu, S. H. Nanostructured Metal Chalcogenides: Synthesis, Modification, and Applications in Energy Conversion and Storage Devices. *Chem. Soc. Rev.* **2013**, *42*, 2986−3017.

(5) Esposito, D. V.; Hunt, S. T.; Stottlemyer, A. L.; Dobson, K. D.; McCandless, B. E.; Birkmire, R. W.; Chen, J. G. Low-Cost Hydrogen-Evolution Catalysts Based on Monolayer Platinum on Tungsten Monocarbide Substrates. *Angew. Chem., Int. Ed.* **2010**, *49*, 9859−9862.

(6) Subbaraman, R.; Tripkovic, D.; Strmcnik, D.; Chang, K. C.; Uchimura, M.; Paulikas, A. P.; Stamenkovic, V.; Markovic, N. M. Enhancing Hydrogen Evolution Activity in Water Splitting by Tailoring Li^+-$Ni(OH)_2$-Pt Interfaces. *Science* **2011**, *334*, 1256−1260.

(7) Parsons, R. The Rate of Electrolytic Hydrogen Evolution and the Heat of Adsorption of Hydrogen. *Trans. Faraday Soc.* **1958**, *54*, 1053−1063.

(8) Huber, G. W.; Shabaker, J. W.; Dumesic, J. A. Raney Ni-Sn Catalyst for H_2 Production from Biomass-Derived Hydrocarbons. *Science* **2003**, *300*, 2075−2077.

(9) Jović, V. D.; Lačnjevac, U.; Jović, B. M.; Karanović, Lj.; Krstajić, N. V. Ni-Sn Coatings as Cathodes for Hydrogen Evolution in Alkaline Solution. Chemical Composition, Phase Composition and Morphology Effects. *Int. J. Hydrogen Energy* **2012**, *37*, 17882−17891.

(10) Jović, B. M.; Lačnjevac, U. Č.; Krstajić, N. V.; Jović, V. D. Ni-Sn Coatings as Cathodes for Hydrogen Evolution in Alkalinesolutions. *Electrochim. Acta* **2013**, *114*, 813−818.

(11) Yamashita, H.; Yamamura, T.; Yoshimoto, K. The Relation Between Catalytic Ability for Hydrogen Evolution Reaction and Characteristics of Nickel-Tin Alloys. *J. Electrochem. Soc.* **1993**, *140*, 2238−2243.

(12) Vijayakumar, J.; Mohan, S.; Anand Kumar, S.; Suseendiran, S. R.; Pavithra, S. Electrodeposition of Ni-Co-Sn Alloy from Choline Chloride-Based Deep Eutectic Solvent and Characterization as Cathode for Hydrogen Evolution in Alkaline Solution. *Int. J. Hydrogen Energy* **2013**, *38*, 10208−10214.

(13) Krstajić, N. V.; Jović, V. D.; Karanović, Lj.; Jović, B. M.; Antozzi, A. L.; Martelli, G. N. Electrodeposition of Ni-Mo Alloy Coatings and their Characterization as Cathodes for Hydrogen Evolution in Sodium Hydroxide Solution. *Int. J. Hydrogen Energy* **2008**, *33*, 3676−3687.

(14) Brown, D. E.; Mahmood, M. N.; Man, M. C.; Turner, A. K. Preparation and Characterization of Low Overvoltage Transition Metal Alloy Electrocatalysts for Hydrogen Evolution in Alkaline Solutions. *Electrochim. Acta* **1984**, *29*, 1551−1556.

(15) Nocera, D. G. The Artificial Leaf. *Acc. Chem. Res.* **2012**, *45*, 767−776.

(16) Dulle, J.; Nemeth, S.; Skorb, E. V.; Irrgang, T.; Senker, J.; Kempe, R.; Fery, A.; Andreeva, D. V. Sonochemical Activation of Al/Ni Hydrogenation Catalyst. *Adv. Funct. Mater.* **2012**, *22*, 3128−3135.

(17) Raj, I. A.; Vasu, K. I. Transition Metal-Based Cathodes for Hydrogen Evolution in Alkaline Solution: Electrocatalysis on Nickel-Based Ternary Electrolytic Codeposits. *J. Appl. Electrochem.* **1992**, *22*, 471−477.

(18) Gong, M.; Li, Y.; Wang, H.; Liang, Y.; Wu, J. Z.; Zhou, J.; Wang, J.; Regier, T.; Wei, F.; Dai, H. An Advanced Ni-Fe Layered Double Hydroxide Electrocatalyst for Water Oxidation. *J. Am. Chem. Soc.* **2013**, *135*, 8452−8455.

(19) Popczun, E. J.; McKone, J. R.; Read, C. G.; Biacchi, A. J.; Wiltrout, A. M.; Lewis, N. S.; Schaak, R. E. Nanostructured Nickel Phosphide as an Electrocatalyst for the Hydrogen Evolution Reaction. *J. Am. Chem. Soc.* **2013**, *135*, 9267−9270.

(20) Liu, P.; Rodriguez, J. A.; Takashiri, Y.; Nakamura, K. Water-Gas-Shift Reaction on a $Ni_2P(001)$ Catalyst: Formation of Oxy-phosphides and Highly Active Reaction Sites. *J. Catal.* **2009**, *262*, 294−303.

(21) Gao, M. R.; Lin, Z. Y.; Zhuang, T. T.; Jiang, J.; Xu, Y. F.; Zheng, Y. R.; Yu, S. H. Mixed-Solution Synthesis of Sea Urchin-Like NiSe Nanofiber Assemblies as Economical Pt-Free Catalysts for Electrochemical H_2 Production. *J. Mater. Chem.* **2012**, *22*, 13662−13668.

(22) Nishikawaa, K.; Dokkob, K.; Kinoshitaa, K.; Wooa, S. W.; Kanamuraa, K. Three-Dimensionally Ordered Macroporous Ni-Sn Anode for Lithium Batteries. *J. Power Sources* **2009**, *189*, 726−729.

(23) Khorasani-Motlagh, M.; Noroozifar, M.; Ekrami-Kakhki, M. Investigation of the Nanometals (Ni and Sn) in Platinum Binary and Ternary Electrocatalysts for Methanol Electrooxidation. *Int. J. Hydrogen Energy* **2011**, *36*, 11554−11563.

(24) Chou, N. H.; Schaak, R. E. Shape-Controlled Conversion of β-Sn Nanocrystals into Intermetallic *M*-Sn (*M* = Fe, Co, Ni, Pd) Nanocrystals. *J. Am. Chem. Soc.* **2007**, *129*, 7339−7345.

(25) Ehinon, K. K. D.; Naille, S.; Dedryvère, R.; Lippens, P. E.; Jumas, J. C.; Gonbeau, D. Ni_3Sn_4 Electrodes for Li-Ion Batteries: Li-Sn Alloying Process and Electrode/Electrolyte Interface Phenomena. *Chem. Mater.* **2008**, *20*, 5388−5398.

(26) Guo, H.; Zhao, H.; Jia, X. Spherical Sn-Ni-C Alloy Anode Material with Submicro/Micro Complex Particle Structure for Lithium Secondary Batteries. *Electrochem. Commun.* **2007**, *9*, 2207−2211.

(27) Zhang, C. F.; Wu, H.; Guo, Z. P.; Lou, X. W. Synthesis of MoS_2-C One-Dimensional Nanostructures with Improved Lithium Storage Properties. *ACS Appl. Mater. Interfaces* **2012**, *4*, 3765−3768.

(28) Kibsgaard, J.; Chen, Z.; Reinecke, B. N.; Jaramillo, T. F. Engineering the Surface Structure of MoS_2 to Preferentially Expose Active Edge Sites for Electrocatalysis. *Nat. Mater.* **2012**, *11*, 963−969.

(29) Wang, J.; Wang, K.; Wang, F. B.; Xia, X. H. Bioinspired Cu Catalyst Effective for Both Reduction and Evolution of Oxygen. *Nat. Commun.* **2014**, *5*, 5285 DOI: 10.1038/ncomms6285.

DOI: 10.1021/acsami.5b00873
ACS Appl. Mater. Interfaces 2015, 7, 9098−9102